# The reliability of atomic data used for oxygen abundance determinations

**C. Mendoza** (IVIC/CeCalCULA, Venezuela)

Contributions from
Efraín Gatuzz (IVIC, Venezuela)
Javier García (U Maryland, USA)
Tim Kallman (NASA-GSFC, USA)
Mike Witthoeft (NASA-GSFC, USA)
Manuel Bautista (WMU, USA)
Nigel Badnell (U Strathcyde, UK)
Franck Delahaye (Obs. Paris, France)
Claude Zeippen (Obs. Paris, France)
Patrick Palmeri (U Mons, Belgium)
Pascal Quinet (U Mons, Belgium)



**Mapping Oxygen in the Universe**
Instituto de Astrofísica de Canarias
15 May 2012

# In the XSTAR fit of the Chandra spectrum towards XTE J1817-330, noticeable $\Delta\lambda$ are found for K lines in O I – O VII

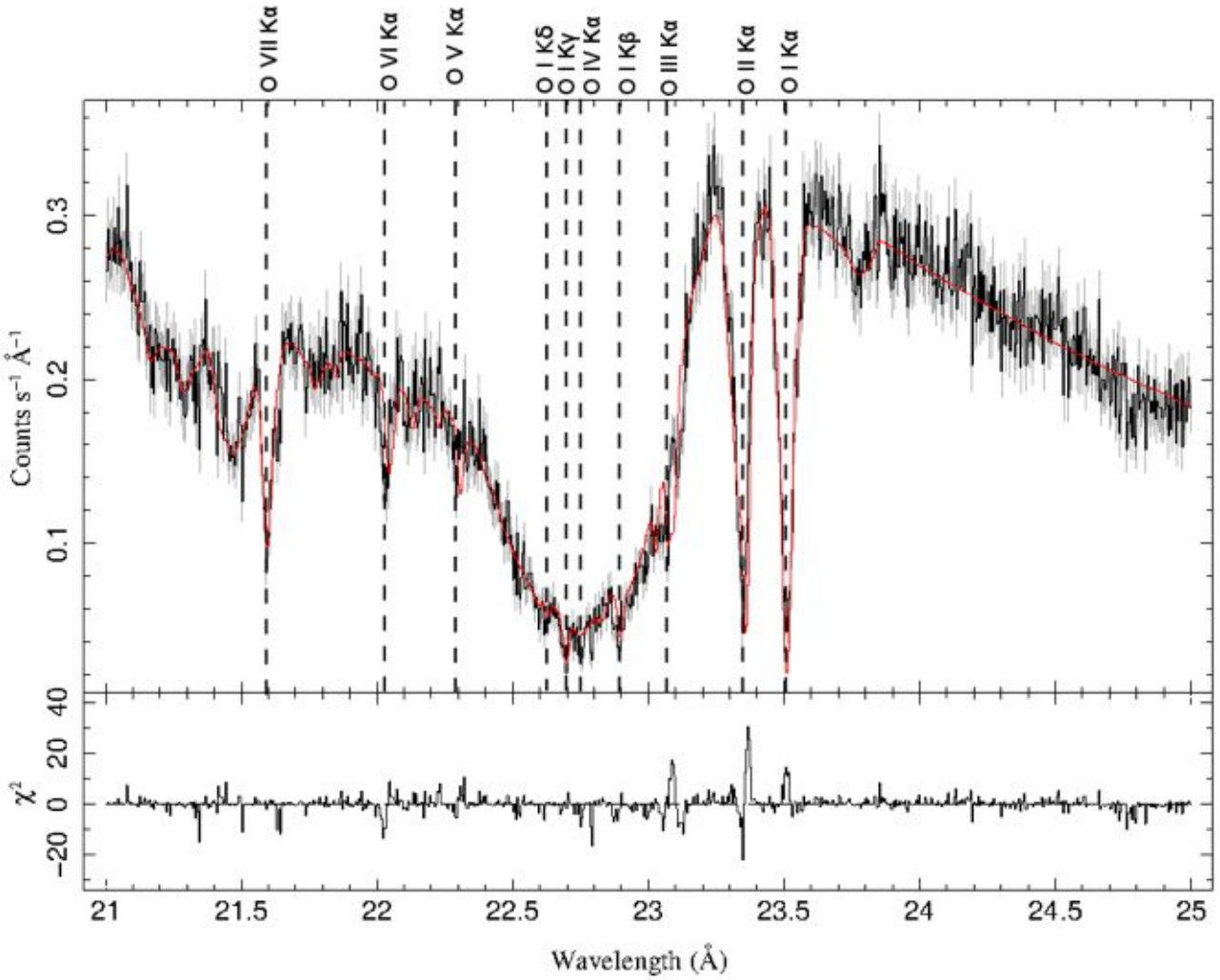

# In the XSTAR fit of the Chandra spectrum towards XTE J1817-330, noticeable $\Delta\lambda$ are found for K lines in O I – O VII

| Ion | Trans. | $\lambda$(Obs) | $\lambda$(XSTAR) | $\Delta\lambda$ |
|---|---|---|---|---|
| O I | 1s–2p | 23.5156 | 23.4886 | -0.027 |
| O II | 1s–2p | 23.3581 | 23.3825 | 0.024 |
| O III | 1s–2p | 23.0706 | 23.1304 | 0.060 |
| O I | 1s–3p | 22.9041 | 22.9143 | 0.010 |
| O IV | 1s–2p | 22.7509 | 22.7741 | 0.023 |
| O I | 1s–4p | 22.7052 | 22.7067 | 0.002 |
| O I | 1s–5p | 22.6242 | 22.6432 | 0.019 |
| O V | 1s–2p | 22.2973 | 22.4185 | 0.121 |
| O VI | 1s–2p | 22.0353 | 22.0078 | -0.027 |
| O VII | 1s–2p | 21.6033 | 21.61 | 0.007 |

# Calculated X-ray wavelengths cannot match spectroscopy accuracy although experimental misassignments are sometimes encountered

**Table A.5.** Comparison of EBIT and theoretical wavelengths (Å) for O K lines.

| Ion | Lower level ($J$) | Upper level ($J'$) | EBIT | Theory |
|---|---|---|---|---|
| O VI | $1s^2 2s(1/2)$ | $1s2s2p(1/2, 3/2)$ | $22.0194(16)^a$ | $22.00^c$ |
| | | | $22.374(8)^b$ | $22.05^d$ |
| | | | | $22.03^e$ |
| O V | $1s^2 2s^2(0)$ | $1s2s^2 2p(1)$ | $22.374(3)^a$ | $22.33^c$ |
| | | | $22.370(10)^b$ | $22.35^d$ |
| | | | | $22.37^e$ |
| O IV | $1s^2 2s^2 2p(1/2, 3/2)$ | $1s2s^2 2p^2(1/2, 3/2)$ | $22.741(5)^b$ | $22.78^c$ |
| | | | | $22.73^d$ |
| | | | | $22.75^e$ |
| O III | $1s^2 2s^2 2p^2(1, 2)$ | $1s2s^2 2p^3(1)$ | $22.071(6)^b$ | $23.08^c$ |
| | | | | $23.05^d$ |
| | | | | $23.07^e$ |

[a] EBIT measurement (Schmidt *et al.* 2004). [b] EBIT measurement (Gu *et al.* 2005). [c] HULLAC calculation (Behar & Kahn 2002). [d] *R*-matrix calculation (Pradhan *et al.* 2003). [e] HFR calculation (García *et al.* 2005).

Table from Grazyna et al. (2012)

# X-ray K lines appear as resonances in the photoionization cross sections

Figure from
García et al (2005)

Kα lines

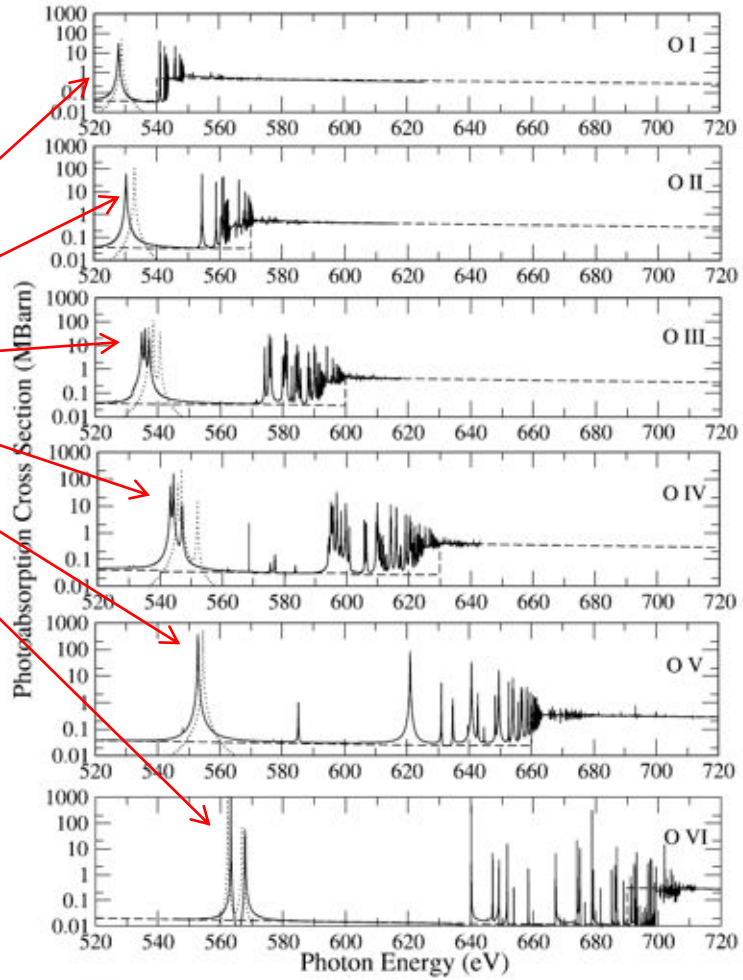


FIG. 5.—High-energy photoionization cross sections of O ions showing the structure of the K edge: *solid curve*, RM1; *dotted curve*, Pradhan et al. (2003); *dashed curve*, Reilman & Manson (1979).

# Radiative data for both b-b and b-f transitions are computed with the R-matrix method

In the *close-coupling approximation* the wave function for the target + $e^-$ system is expanded in terms of the target eigenfunctions:

$$\Psi(J\pi) = \mathcal{A}\sum_i \chi_i \frac{F_i(r)}{r} + \sum_j c_j \Phi_j \qquad (1)$$

where $\chi_i$ are the target eigenfunctions. The functions $\Phi_j$ are bound-type functions of the total system built with target orbitals.

Solutions are obtained with the *R*-matrix method (Burke et al 1971; Berrington et al. 1974, 1978, 1987; Seaton 1985)

# Theoretical fine tuning relies on accurate laboratory measurements

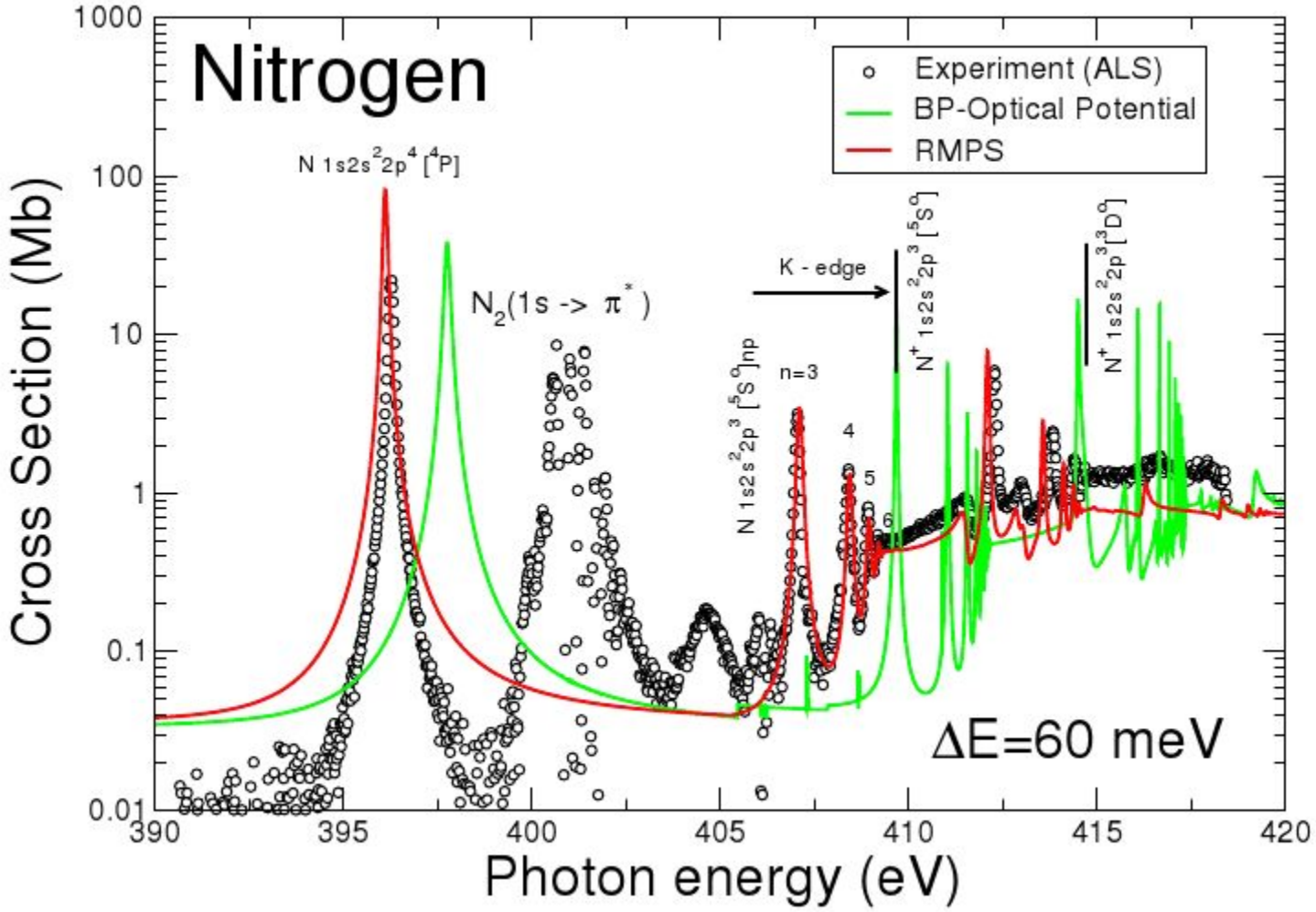


Experiment and RMPS: Sant'Anna et al (2011)
BP-optical potential: García et al (2009)

# Decay of K-vacancy states in O ions is dominated by Auger spectator channels

When a photon promotes a K-shell electron to an excited Rydberg state

$$h\nu + 1s^2 2s^\lambda 2p^\mu \longrightarrow 1s2s^\lambda 2p^\mu np\ , \tag{2}$$

it decays via the radiative and Auger manifold

$$1s2s^\lambda 2p^\mu np \xrightarrow{Kn} 1s^2 2s^\lambda 2p^\mu + h\nu_n \tag{3}$$

$$\xrightarrow{K\alpha} 1s^2 2s^\lambda 2p^{\mu-1} np + h\nu_\alpha \tag{4}$$

$$\xrightarrow{KLn} \begin{cases} 1s^2 2s^\lambda 2p^{\mu-1} + e^- \\ 1s^2 2s^{\lambda-1} 2p^\mu + e^- \end{cases} \tag{5}$$

$$\xrightarrow{KLL} \begin{cases} 1s^2 2s^\lambda 2p^{\mu-2} np + e^- \\ 1s^2 2s^{\lambda-1} 2p^{\mu-1} np + e^- \\ 1s^2 2p^{\mu-2} np + e^-\ . \end{cases} \tag{6}$$

The decay is dominated by the KLL channels (6) where the *np* electron remains a spectator. As $n \to n_{\max}$, the KLL channels must include target states with $2 \le n \le n_{\max}$ which become intractable in the standard R-matrix method as $n_{\max} \to \infty$, but can be treated with an optical potential (Robicheaux et al. 1995; Gorczyca & Badnell 1996, 2000).

# Auger damping leads to resonances with constant widths and a smearing of the K edge

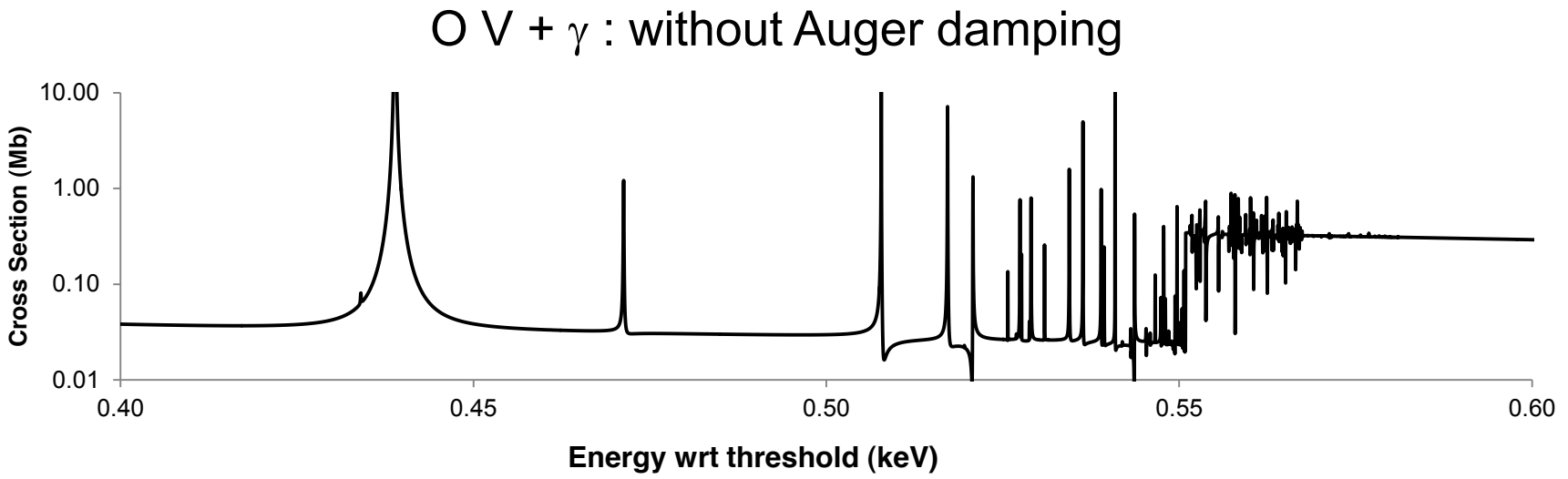


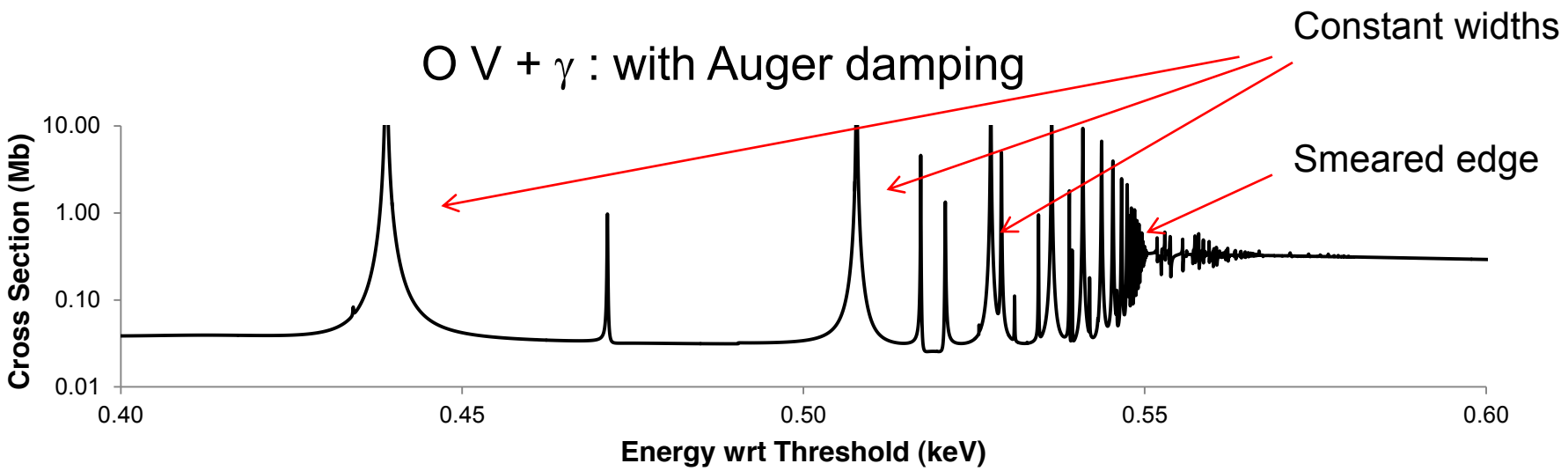

# Damping leads to a more populated and smeared K-edge structure

Fe K-edge structures computed by Palmeri et al. (2002)

Kα array

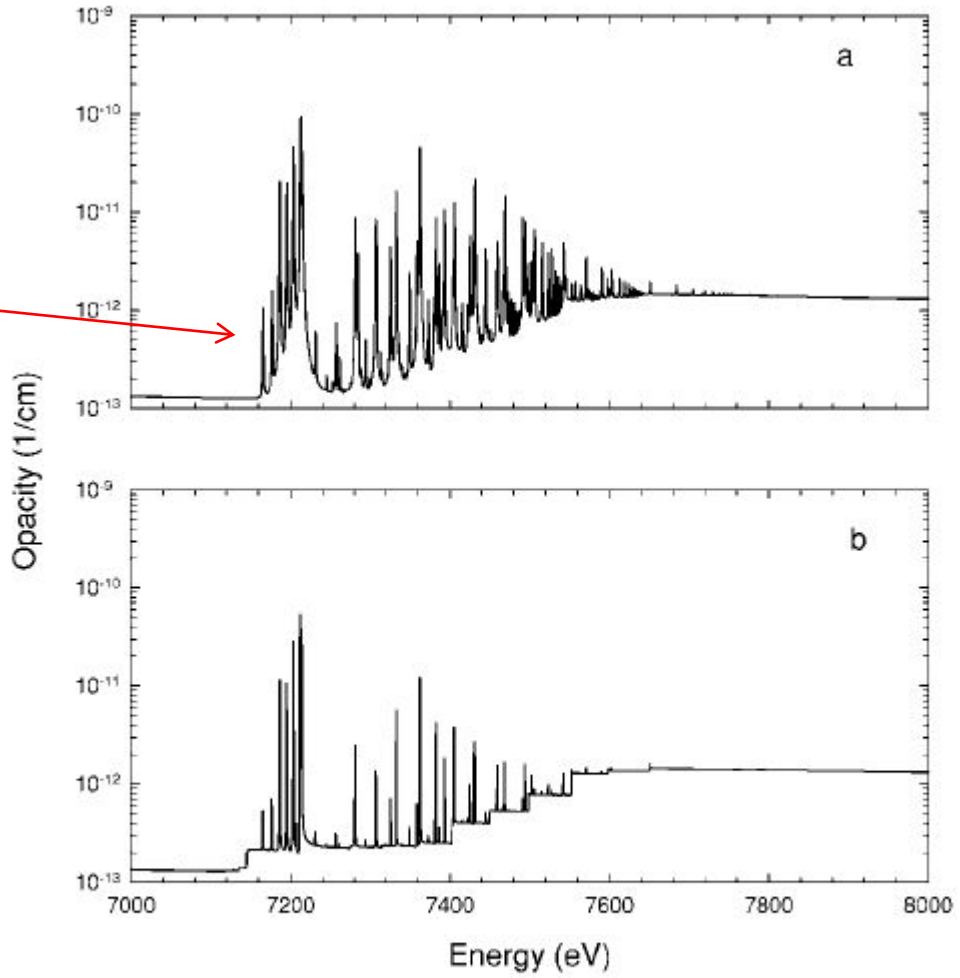


FIG. 3.—Opacities for a photoionized gas with solar elemental abundances and $\xi = 10$, including (*a*) K damped photoionization cross sections and (*b*) undamped cross sections.

# Within the OP, inner-shell contributions were not estimated with the R-matrix method but with an atomic structure code (AUTOSTRUCTURE)

Figure from
Badnell et al. (2005)

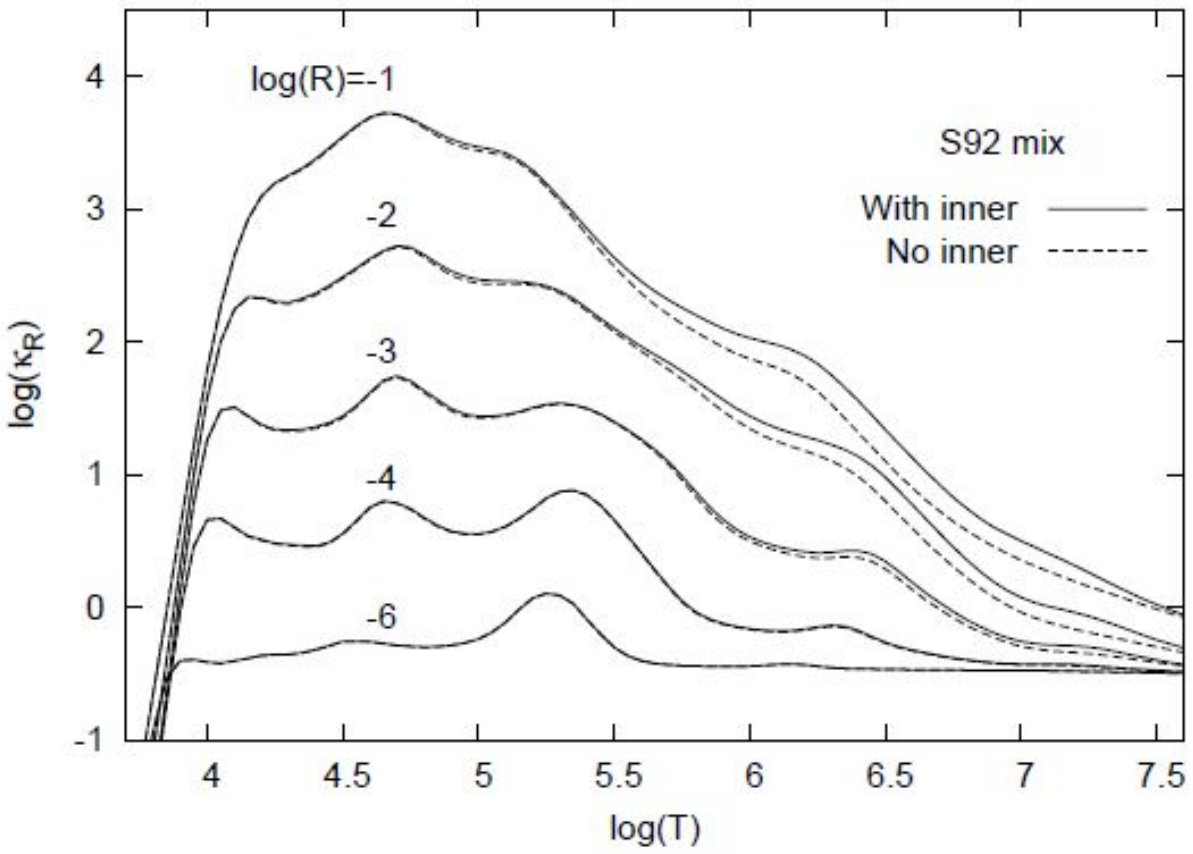


**Figure 1.** Rosseland-mean opacities from OP for S92 mix, with and without inner-shell contributions.

# By considering the photoionization cross sections of Fe XVII, Nahar et al. (2011) have asserted that the solar opacities are underestimated

Figure from
Nahar et al. (2011)

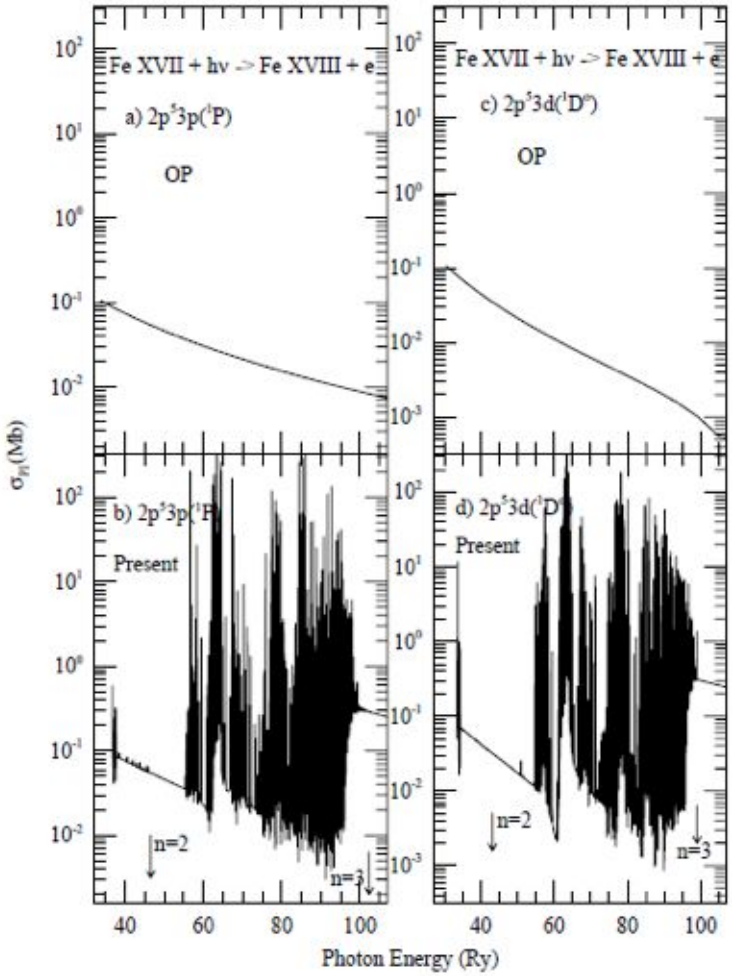

# K photoabsorption of O V $1s^2 2sns$ with n=2 Li-like target. We see satellite lines

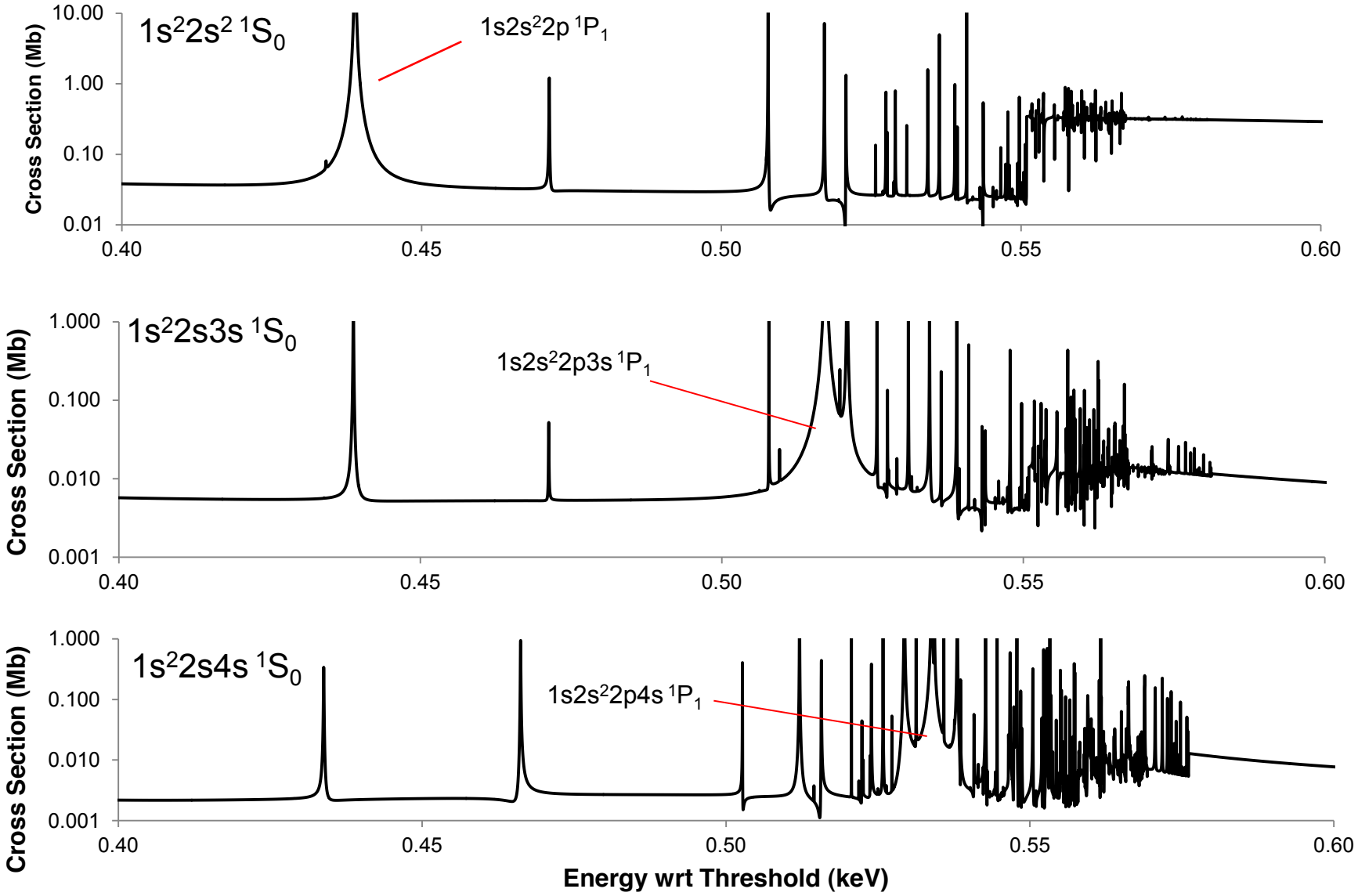

# K photoabsorption of O V $1s^2 2s3s\ ^1S$ with two targets. We see a "satellite K edge" in the 2nd

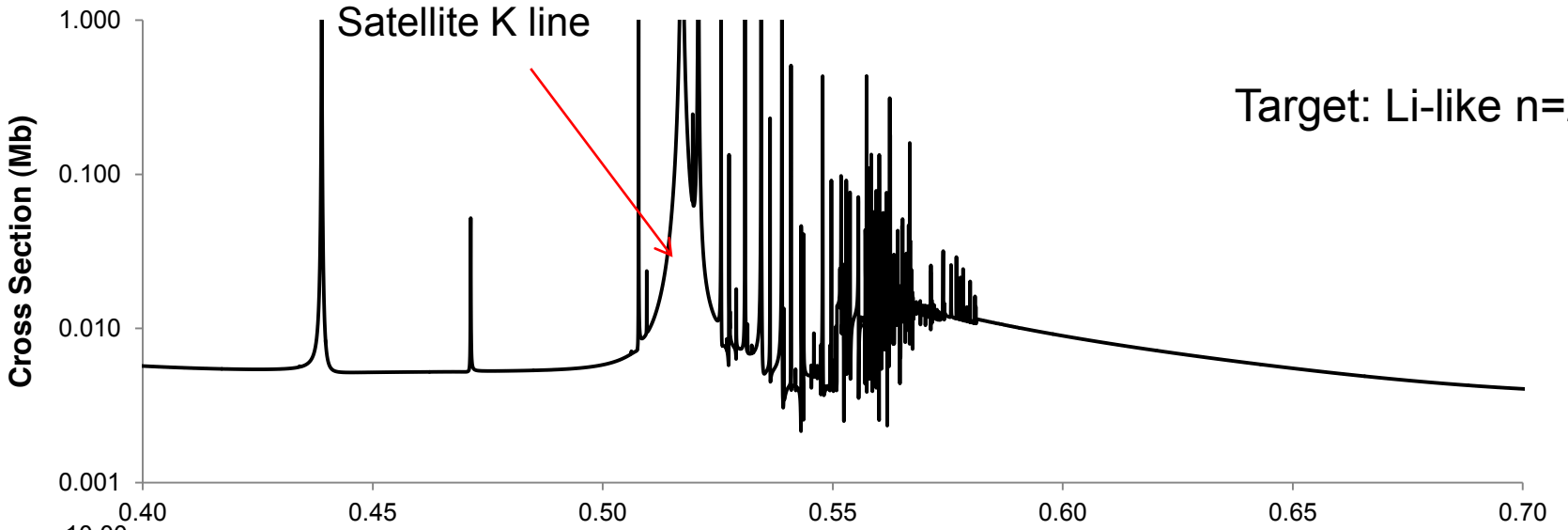


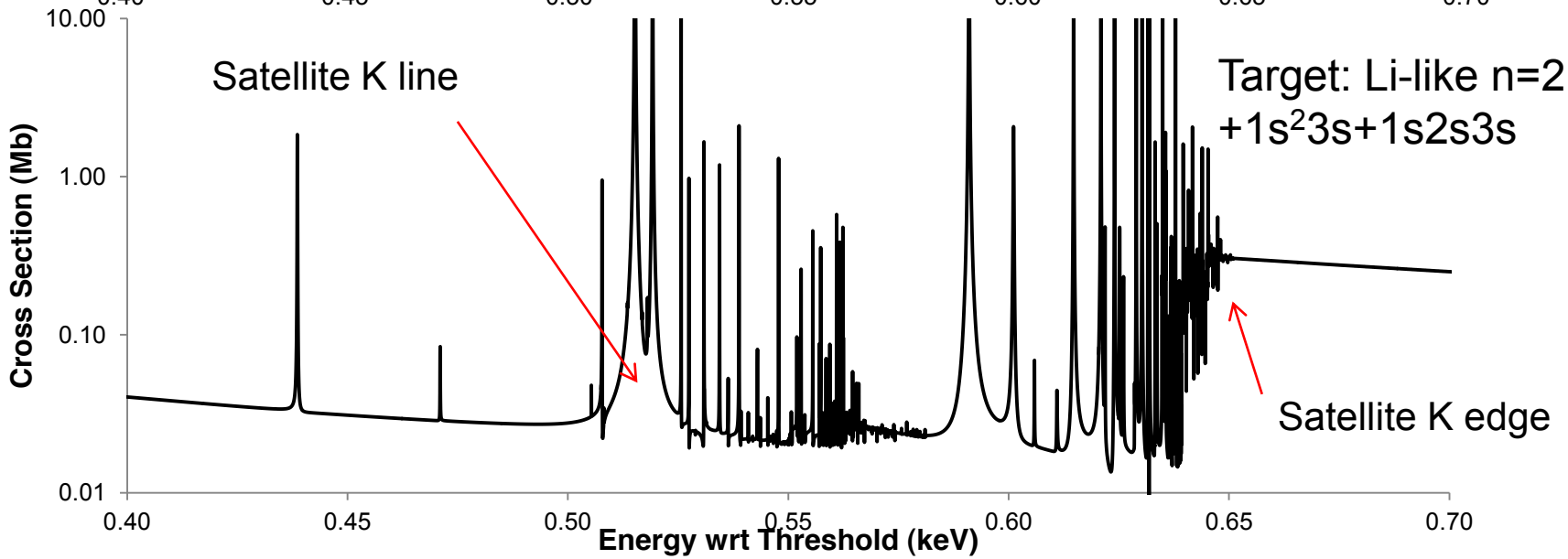

# The R-matrix method cannot be used for rendering the satellite K edges for high n states

In order to represent the K absorption of an $1s^2 2s n\ell$ state in a Be-like ion, say,

$$1s^2 2s n\ell + \gamma \longrightarrow 1s2s n\ell + e^- \ , \qquad (7)$$

the Li-like target states $1s^2 n'\ell$ and $1s2s n'\ell$ $(2 \leq n' \leq n)$ must be included in the close-coupling expansion (1) in order to obtain its "satellite K edge" structure. This is numerically intractable in the R-matrix method for high $n$.

# For computing both radiative and collisional data for CELs, two effects must be considered

To compute radiative or collisional data for CEL, two effects must be considered in detail:

1. Electron correlation: configuration interaction, close-coupling
2. Relativistic effects:
   - Pauli Hamiltonian

$$H_{\mathrm{BP}} = H_{\mathrm{NR}} + H_{\mathrm{1B}} \tag{8}$$

where the one-body relativistic operators

$$H_{\mathrm{1B}} = \sum_{n=1}^{N} f_n(\mathrm{mass}) + f_n(\mathrm{D}) + f_n(\mathrm{so}) \tag{9}$$

represent the spin–orbit interaction, $f_n(\mathrm{so})$, the mass variation, $f_n(\mathrm{mass})$, and the one-body Darwin correction, $f_n(\mathrm{D})$.

   - Breit–Pauli Hamiltonian

$$H_{\mathrm{BP}} = H_{\mathrm{NR}} + H_{\mathrm{1B}} + H_{\mathrm{2B}}, \tag{10}$$

   - Fully relativistic (Dirac–Fock)

# Both e-correlation and RE are important for line ratios of forbidden lines

Table A.1. *A*-value ratios for forbidden lines in the ground configuration of O ions.

| Ion | Parameter | TFF | GMZ | SZ | Z | Obs | Lab | WL |
|---|---|---|---|---|---|---|---|---|
| O I | $A(^1D_2 - {}^3P_2)$ | 6.503E−3 | 6.535E−3 | 6.446E−3 | | | | 6300 |
| | $A(^1D_2 - {}^3P_1)$ | 2.101E−3 | 2.111E−3 | 2.151E−3 | | | | 6364 |
| | Ratio | 3.10 | 3.10 | 3.00 | | 2.997(16) | | |
| | $A(^1S - {}^1D)$ | 1.260E+0 | 1.124E+0 | | | | | 5577 |
| | $A(^1S - {}^3P)$ | 7.877E−2 | 7.940E−2 | | | | | 2972 |
| | Ratio | 16.0 | 14.2 | | | 9.3(5) | 18.6 | |
| O II | $A(^2D_{5/2} - {}^4S^o_{3/2})$ | 4.123E−5 | | | 3.588E−5 | | | 3729 |
| | $A(^2D_{3/2} - {}^4S^o_{3/2})$ | 1.635E−4 | | | 1.810E−4 | | | 3726 |
| | Ratio | 0.252 | | | 0.198 | | | |
| O III | $A(^1D_2 - {}^3P_2)$ | 2.028E−2 | 2.041E−2 | 2.046E−2 | | | | 5007 |
| | $A(^1D_2 - {}^3P_1)$ | 6.951E−3 | 6.995E−3 | 6.791E−3 | | | | 4959 |
| | Ratio | 2.92 | 2.92 | 3.01 | | | 3.00(8) | |

TFF: Tachiev & Froese Fischer (2001, 2002). GMZ: Galavís *et al.* (1997). SZ: Storey & Zeippen (2000). Z: Zeippen (1987).

Obs: terrestrial nightglow observations (Sharpee & Slanger 2006, Gattinger et al. 2009)
Lab: Laboratory measurements

Table from Grazyna et al. (2012)

# The near-threshold resonance structure can be sensitive to relativistic effects

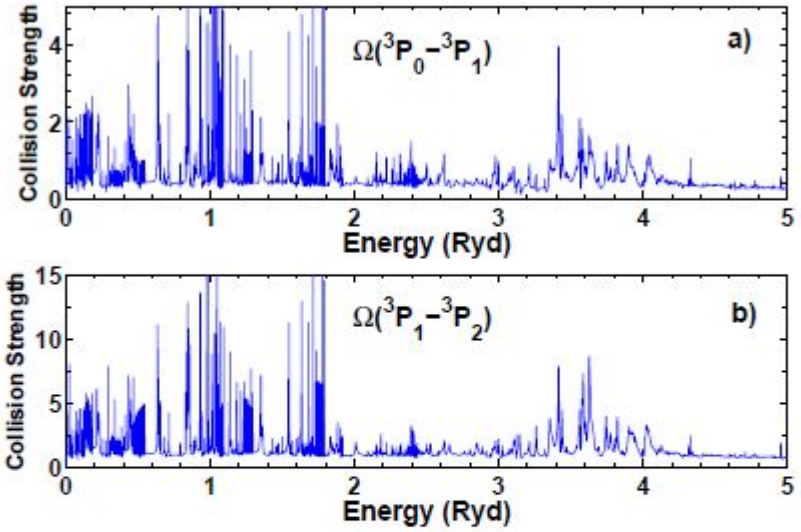


**Figure 1.** Collision strengths for the ø3 IR fine structure transitions $2p^2(^3P_0 - ^3P_1, ^3P_1 - ^3P_2)$ at $\lambda\lambda$ a) 88 $\mu$m and b) 52 $\mu$m respectively. High resolution at near-threshold energies is necessary for accuracy in rate coefficients at low temperatures. The top panel shows an expanded view in the region E $\leqslant$ 1 Rydberg; both transitions have similar resonance structures.

Recent results on forbidden lines of O III by Palay et al (2012)

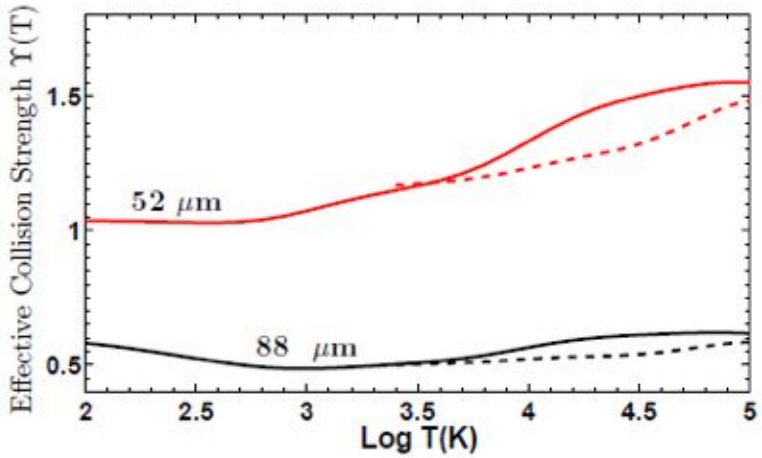


**Figure 2.** Maxwellian averaged effective collision strengths $\Upsilon(T)$ (Eq. 1) for the transitions $^P_0 - ^3P_1$ at 88 $\mu$m and $^3P_1 - ^3P_2$ at 52 $\mu$m (solid lines, c.f. Fig. 1). Previous results without relativistic (1) effects (Aggarwal and Keenan 1999) are also shown (dashed lines) in the temperature range available $T_e \geqslant$ 2500 K.

# The near-threshold resonance structure can be sensitive to relativistic effects

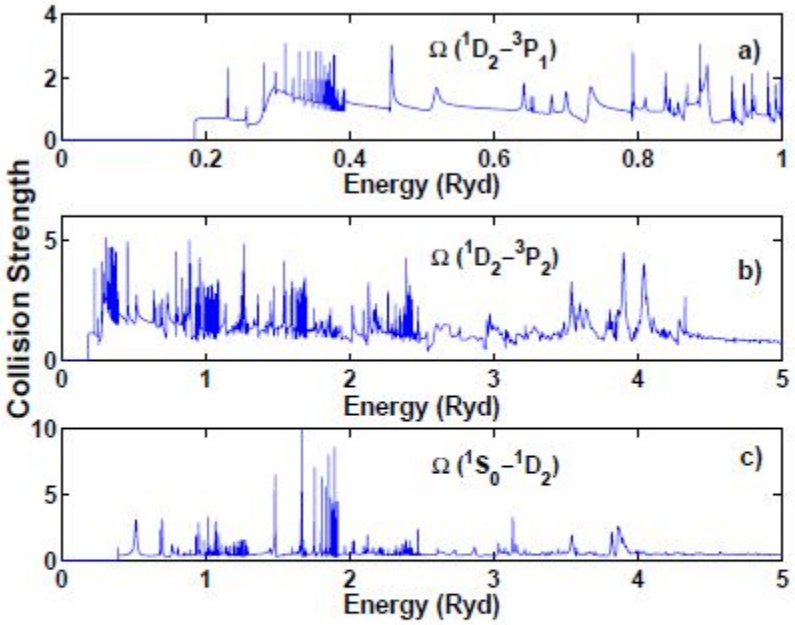


**Figure 4.** Collision strengths of the ø3 optical transitions. The two transitions $^1D_2 - ^3P_1, ^1D_2 - ^3P_2$ in a) and b) have similar resonance structures; the top panel a) presents an expanded view below E $\leqslant$ 1 Rydberg.

Recent results on forbidden lines of O III by Palay et al (2012)

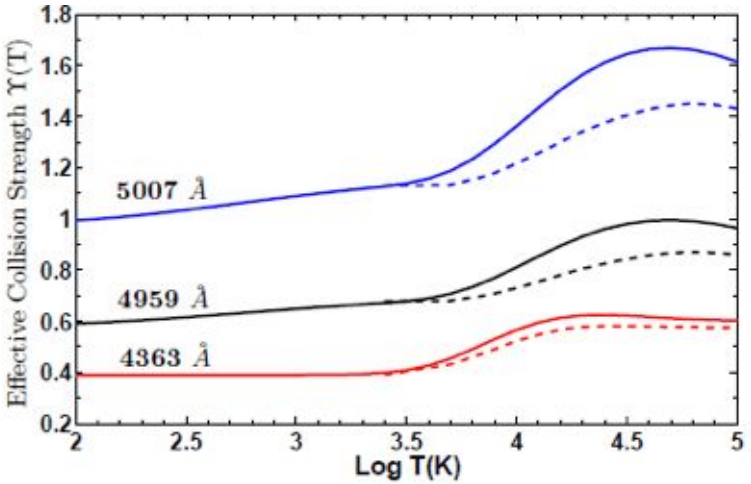


**Figure 5.** Effective collision strengths of the ø3 optical transitions $^1D_2 - ^3P_1, ^1D_2 - ^3P_2, ^1S_0 - ^1D_2$ at λλ 4959, 5007 and 4363 respectively (c.f. Fig. 4).

# Diagnostics based on line ratios can be sensitive to the atomic model

$R1 = I(787.72\ \text{Å})/I(279.93\ \text{Å})$
$R2 = I(554.51\ \text{Å})/I(279.93\ \text{Å})$
$R3 = I(787.72\ \text{Å})/I(554.51\ \text{Å})$
$R4 = I(787.72\ \text{Å})/I(b790\ \text{Å})$

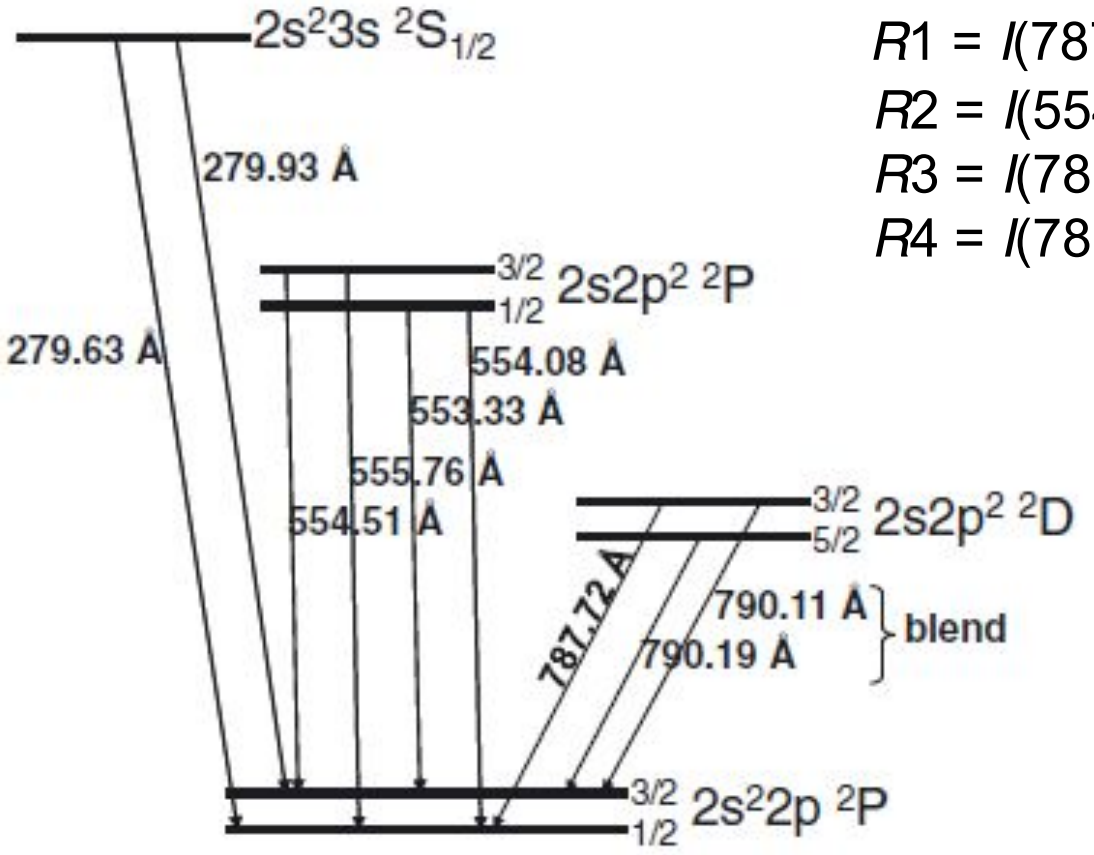


**Fig. 1.** Partial level diagram for O IV.

Figure from Palay et al (2012)

# Diagnostics based on line ratios can be sensitive to the atomic model

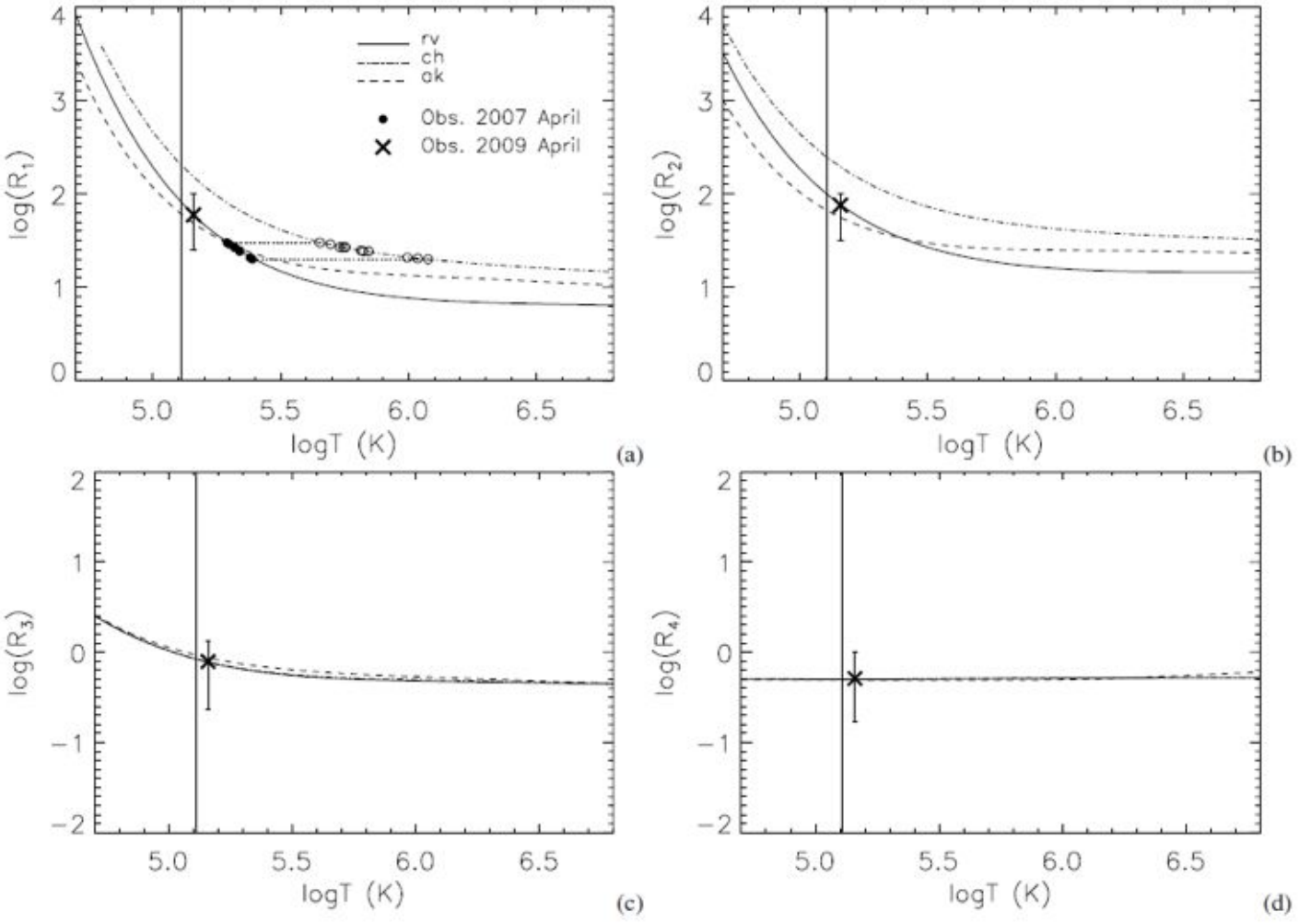


Figure from Palay et al (2012)

# Regarding ORLs, we can say two things:

- Although some authors (e.g. Nahar et al. 2010 and Xuan Fang, next talk, for O II) have found that the low-temperature dielectronic rates are enhanced by a well-resolved IC resonance structure, the CEL/ORL discrepancy has not disappeared.
- In spite of considerable effort on our part, databases do not list the raw collision strengths or photoionization cross sections in order to compute rates for non-Maxwellian or kappa distributions (see talk by David Nicholls)

# Conclusions

- Theoretical wavelengths cannot match spectroscopic accuracy, and fine tuning relies on measurement availability
- The relevance of laboratory astrophysics is beginning to be appreciated by funding agencies, and a closer synergy between theoreticians and experimentalists would help
- K edge photoabsorption of excited  levels gives rise to “satellite K edges” which have not been treated in detail in opacity calculations, and could certainly lead to increases in the O and Fe RMOs in the conditions associated with the base of the convection zone
- The inclusion of both electron correlation and relativistic effects in the computation of both radiative and collisional data for CELs still leads to significant differences
- There are database problems relating to the availability of the raw collision strengths in order to determine rates for non-Maxwellian electron distributions